# RADIO FREQUENCY TOMOGRAPHY IN MOBILE NETWORKS

*Benjamin R. Hamilton, Xiaoli Ma*

Georgia Institute of Technology
Dept. of Electrical and Computer Eng.
Atlanta, GA

*Robert J. Baxley, Stephen M. Matechik*

Georgia Tech Research Institute
Information and Communications Laboratory
Atlanta, GA

## ABSTRACT

Networks of portable wireless devices have shown enormous promise in improving communications and sensing capabilities in a large number of important applications. While much work has focused on using specialized sensors to obtain information about the physical environment, we examine the problem of exploiting the received signal strength (RSS) measurements already being used for ad-hoc networking. We describe how information about the shadowing environment is encoded into RSS measurements and present the novel RF Exploitation for Tomographic Imaging and Non-cooperative Analysis (RETINA) algorithm to detect stationary obstacles and track moving objects. We compare this algorithm with existing methods through analysis and simulation and show that RETINA achieves significantly higher accuracy.

***Index Terms***— Tomography, ad-hoc networking, mobility, Kalman filtering

## 1. INTRODUCTION

Self-organizing ad hoc networks promise a revolution in communications with increased flexibility and reliability and reduced deployment and maintenance costs. Additionally the development of minituarized sensing technologies have allowed for the collection of unparalled amounts of sensing data. The combination of both communications and sensing technologies shows promise in applications ranging from intrusion detection to environmental monitoring [1]. While there has been a significant amount of research done on the collection and analysis of conventional sensing techniques, the sensing capabilities of the wireless network itself have received less interest.

In dense networks with large numbers of wireless devices, the received signal strength (RSS) measurements between all the wireless nodes in the network contain a significant amount of information about the environment the network is in. As radio transmissions pass through the environment, the signal is attenuated by the objects it passes through, causing shadowing. With appropriate signal processing, these deviations in signal strength from a free-space model can be used to determine the contribution of each point in the network area to the measured shadowing. Since the shadowing is caused by the attenuation of radio signals as it passes through objects, this effectively provides a method for through-wall detection and tracking of both static and moving objects. This capability has compelling applications ranging from surveillance to locating survivors in rescue operations.

Although techniques using radio signals for imaging have been used in geophysics for some time [2,3], these methods only consider the situation where scattering and reflective effects are significant. In order to reconstruct the image, they require the phase information from the received signal and solve the discretized wave equation. These methods have extremely high computational complexity and cannot achieve real-time imaging.

Recent works have instead focused on a simpler system which has fewer of these scattering and reflective effects so that the reconstruction can be greatly simplified. It has been shown that for these cases, the image reconstruction is similar to the tomography problem, which can be solved by known techniques such as filtered backprojection [4]. Such techniques were first applied to imaging the shadowing elements in networks of simple wireless devices in [5]. In the works that followed [6, 7], Wilson et al investigated methods of detecting motion or changes in the environment with radio frequency (RF) tomography techniques. These algorithms do not attempt to image the static elements of the network area and do not consider the situation where some of the nodes in the network may be mobile.

The reconstructed images from RF tomography differ from the channel gain maps produced by some algorithms for cognitive radio [8] since the channel gain maps show the channel gain from each node to every point in the network area. This means that there is a map for each node in the network, and these maps do not show the location of attenuating objects in the network area without processing using a tomographic reconstruction algorithm such as those discussed in this paper. Additionally, these techniques can not be applied when the cognitive radio nodes are mobile.

In this paper we present the RF Exploitation for Tomographic Imaging and Non-cooperative Analysis (RETINA) algorithm. We present an analytical comparison of this algorithm with existing methods and show that it is more flexible and more accurate. We then verify this analytical result through simulation.

### 1.1. Problem Statement

The problem is to estimate the contribution of each point in space to the shadowing present in a series of measurements. We assume a single-path channel between two nodes with both shadowing and path loss. This model can be extended to multi-path channels if only the first arriving path is considered, and the other delayed paths treated as noise. The transmitted signal $x$ is received as:

$$y = hx + u, \tag{1}$$

This research was sponsored (in part) by the Air Force 46th Test Systems Support Squadron, Eglin AFB, FL under the Command, Control, Communications, Computer, Intelligence (C4I), and Munitions Test Improvement Contract III (CIMTIC III).

978-1-4673-0183-1/12/$31.00 ©2012 IEEE

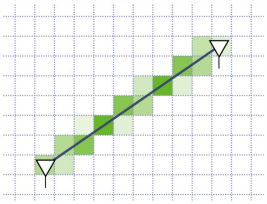

**Fig. 1**. Example SLF weights

where $h$ is the wireless channel and $u$ is additive white Gaussian noise (AWGN) with variance $\sigma_u^2$. The channel $h$ is

$$h = 10^{\frac{z}{20}} d^{-\alpha}, \tag{2}$$

where $d$ is the distance between transmitter and receiver, $\alpha$ is the path loss exponent (nominally between 2 and 4), and $z$ is the shadowing component.

While there are a large number of shadowing models currently in use [8–11], we consider a shadowing model where the shadowing is the vector product of a weight vector $\boldsymbol{b}$ and a spatial loss field (SLF) $\boldsymbol{g}$:

$$z = \boldsymbol{b}\boldsymbol{g}. \tag{3}$$

The SLF represents the additional attenuation at each point in space. The weight vector is determined as a function of the transmitter and receiver position, and determines how much the SLF at each point in space affects the resulting measurement. A visual example of such weights is shown in Figure 1. A shadowing model with such properties is the NeSh model [12, 13].

Since the shadowing measurement (in dB) between any given pair of transceivers $(A, B)$ is a linear functions of the spatial loss field such that $z_{AB} = \boldsymbol{b}_{AB}\boldsymbol{g}$, we can rewrite this in matrix form as

$$\boldsymbol{z} = \boldsymbol{B}\boldsymbol{g}, \tag{4}$$

where $\boldsymbol{B}$ is a matrix containing the row vectors $\boldsymbol{b}_{AB}$ for all transceivers pairs $(A, B)$ and the vector $\boldsymbol{z}$ contains the corresponding measurements, $z_{AB}$. Then the spatial loss field can be estimated as

$$\hat{\boldsymbol{g}} = \boldsymbol{B}^{-1}\boldsymbol{z}. \tag{5}$$

In most cases, however this inversion is not possible since $\boldsymbol{B}$ is singular. To compensate for this, regularization techniques such as Tikhonov regularization are applied.

### 1.2. Existing works

Wilson et al [6, 7] have investigated the use of RF tomography to detect and track moving objects. This method works by obtaining the windowed variance of the RSS measurements, and projecting this variance back into the image domain. A block diagram is shown in Figure 2.

While this method's ingenious use of statistics on the RSS measurements allows it to see through the noise and artifacts from modeling error it has several limitations. The reliance on RSS measurement statistics means that it cannot be applied in networks where the nodes making the measurements are mobile. Further, the use of the windowed variance means that reconstructed images of the moving objects consist of motion blurs. These blurs begin weakly from the past position at the beginning of the window, reach a maximum value at the middle of the window, and then fade as they approach the moving object's current position. This makes this algorithm less useful for real-time intelligence.

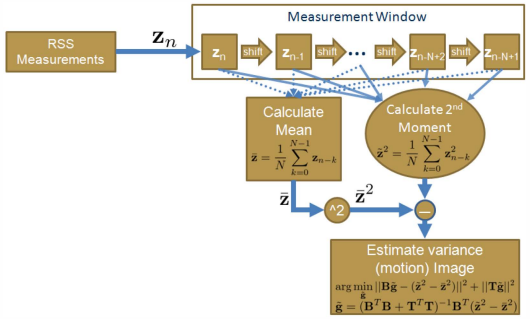


**Fig. 2**. Block diagram of the algorithm in [6]

Although this algorithm was not designed to estimate stationary shadowing components in the network, we will use a small modification which estimates the stationary shadowing based on the windowed mean RSS measurements to facilitate comparison.

## 2. RETINA

In this paper we propose the RF Exploitation for Tomographic Imaging and Non-cooperative Analysis (RETINA) algorithm. RETINA uses a recursive least-squares approach to perform real-time imaging of both the static and dynamic shadowing components in the network area. It uses a motion model to accurately separate and track moving objects in the network area. Because it performs the estimation in the image domain, instead of on the individual measurements, it is able to work when nodes in the network are mobile. Further, the use of the motion model allows for better time resolution of the dynamic shadowing components in the network.

We represent the state of the spatial loss field at time $n$ as a vector $\boldsymbol{\theta}[n]$ containing both the static and dynamic components: $\boldsymbol{\theta}[n] = \begin{bmatrix}\boldsymbol{g}^T & \tilde{\boldsymbol{g}}[n]^T\end{bmatrix}^T$. At each measurement interval $n$, the shadowing measurement $\boldsymbol{z}_n$ is

$$\boldsymbol{z}_n = \begin{bmatrix}\boldsymbol{B}[n] & \boldsymbol{B}[n]\end{bmatrix}\boldsymbol{\theta}[n], \tag{6}$$

where $\boldsymbol{B}[n]$ is the matrix of weight vectors determined according to the shadowing model.

Moving objects in the network area are assumed to move so that the difference between their next and previous position is Gaussian. This is effectively an auto-regressive (AR) position model since the future position of objects is related to the current position $\boldsymbol{s}[n]$ position as

$$\boldsymbol{s}[n+1] = \boldsymbol{s}[n] + \boldsymbol{v}[n], \tag{7}$$

where $\boldsymbol{v}[n]$ is iid Gaussian random vector with mean $\bar{\boldsymbol{v}} = \boldsymbol{0}$ and covariance $\boldsymbol{C}_v = \sigma_v^2\boldsymbol{I}$. This model cannot be directly used, however, since RETINA does not track objects, but instead tracks changes in the spatial loss field induced by such objects.

We can determine the effect on the dynamic image by considering what would happen to a cloud of point-like shadowing objects obeying this AR model. If each point in the cloud has magnitude $a_k$ and position $\boldsymbol{s}_k$, we can write the dynamic continuous spatial loss field from the cloud as a function of position $\boldsymbol{s}$:

$$\tilde{g}(\boldsymbol{s})[n] = \sum_k a_k \delta\left(||\boldsymbol{s} - \boldsymbol{s}_k[n]||\right), \tag{8}$$

where $\delta(x)$ is the Dirac delta function. Since the points in the cloud all follow (7), the continuous spatial loss field at the next time frame

can be written as

$$\tilde{g}(\boldsymbol{s})[n+1] = \sum_k a_k \delta\left(||\boldsymbol{s} - \boldsymbol{s}_k[n] + \boldsymbol{v}_k[n]||\right). \quad (9)$$

If we take the expected value of (9), we find that the average effect of this movement model is to apply a Gaussian smoothing filter (with covariance $\boldsymbol{C}_v$) to the dynamic spatial loss field. Returning to the discrete field $\tilde{\boldsymbol{g}}[n]$, we can write the analogous state equation for dynamic component of the expected spatial loss field as

$$\tilde{\boldsymbol{g}}[n+1] = \boldsymbol{\Gamma}\tilde{\boldsymbol{g}}[n], \quad (10)$$

where $\boldsymbol{\Gamma}$ is the 2-D Gaussian filter operator. We then can find the covariance of this spatial loss field estimate as

$$\boldsymbol{C}_{\tilde{g}}[n] = \boldsymbol{\Gamma}\,\mathrm{diag}(\tilde{\boldsymbol{g}}[n] \circ \tilde{\boldsymbol{g}}[n]) - \boldsymbol{\Gamma}\tilde{\boldsymbol{g}}[n]\tilde{\boldsymbol{g}}[n]^T\boldsymbol{\Gamma}^T, \quad (11)$$

where '$\circ$' denotes the Hadamard (element-wise) matrix product.

Given these state equations, we formulate RETINA based on the well-known Kalman filter [14]. We represent the spatial loss field estimate at time $n$ based on the first $k$ measurements as $\hat{\boldsymbol{\theta}}[n|k]$, and its variance as $\boldsymbol{P}[n|k]$. The Kalman filter consists of two main parts: the measurement update and the state update.

In the measurement update, the current set of measurements $\hat{\boldsymbol{z}}[n]$ is incorporated into the current spatial loss field estimate. For simplicity we define $\boldsymbol{H}[n] = \begin{bmatrix}\boldsymbol{B}[n] & \boldsymbol{B}[n]\end{bmatrix}$ and $\boldsymbol{C}_u = \sigma_u^2\boldsymbol{I}$.

$$\boldsymbol{S}[n] = \boldsymbol{H}[n]\boldsymbol{P}[n|n-1]\boldsymbol{H}[n]^H + \boldsymbol{C}_u \quad (12)$$

$$\boldsymbol{K}[n] = \boldsymbol{P}[n|n-1]\boldsymbol{H}[n]^H\boldsymbol{S}[n]^{-1} \quad (13)$$

$$\hat{\boldsymbol{\theta}}[n|n] = \hat{\boldsymbol{\theta}}[n|n-1] + \boldsymbol{K}[n]\left(\hat{\boldsymbol{z}}[n] - \boldsymbol{H}[n]\hat{\boldsymbol{\theta}}[n|n-1]\right) \quad (14)$$

$$\boldsymbol{P}[n|n] = (\boldsymbol{I} - \boldsymbol{P}[n|n-1]\boldsymbol{H}[n])\,\boldsymbol{P}[n|n-1]. \quad (15)$$

In the state update, the state update matrix $\boldsymbol{F}$ is applied to the previous state $\hat{\boldsymbol{\theta}}[n-1|n-1]$ and the previous mean squared error (MSE) $\boldsymbol{P}[n-1|n-1]$. Writing the forward state operator $\boldsymbol{F}$ as $\boldsymbol{F} = \begin{bmatrix}\boldsymbol{I} & \boldsymbol{0}\\ \boldsymbol{0} & \boldsymbol{\Gamma}\end{bmatrix}$, the state update can be written as:

$$\hat{\boldsymbol{\theta}}[n|n-1] = \boldsymbol{F}\hat{\boldsymbol{\theta}}[n-1|n-1], \quad (16)$$

$$\boldsymbol{P}[n|n-1] = \boldsymbol{F}\boldsymbol{P}[n-1|n-1]\boldsymbol{F}^H + \boldsymbol{C}_w[n], \quad (17)$$

where

$$\boldsymbol{C}_w[n] = \begin{bmatrix}\boldsymbol{0} & \boldsymbol{0}\\ \boldsymbol{0} & \boldsymbol{C}_{\tilde{g}}[n]\end{bmatrix}$$

where $\boldsymbol{C}_{\tilde{g}}[n]$ as in Eq. (11).

A block diagram of the RETINA algorithm is shown in Figure 3.

## 3. PERFORMANCE COMPARISON

We compared the performance of the RETINA algorithm to the modified variance-based algorithm described in Section 1.2 through simulation. The simulation consisted of 28 nodes around a simulated structure with 5 simulated objects moving inside the structure. Both algorithms were configured to estimate the spatial loss field for a 41x41 pixel grid centered on the simulated structure. The true spatial loss field for the structure is shown in Figure 4. The mobile objects were modeled as an additional spatial loss localized around the object's position. This additional spatial loss was in the shape of a small Gaussian with a variance of 1 pixel in size. Measurements were generated from the total spatial loss field using the NeSh model.

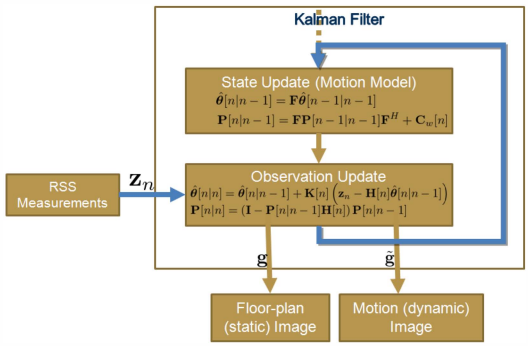


**Fig. 3**. RETINA Block Diagram

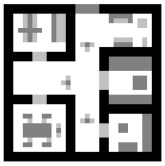

**Fig. 4**. Simulated spatial loss field

In the first simulation, the 28 measuring nodes were stationary and placed along the perimeter of the region. The reconstructed spatial loss fields after 3000 measurement/movement iterations for the variance-based algorithm and RETINA are shown in Figure 5. The filled circles denote the location of the measuring nodes, and the empty circles denote the location of the moving objects.

Comparing Figure 5(a) and Figure 5(c), RETINA achieves comparable accuracy as the variance-based method for estimating the static structure. The reconstruction is not very clear because there are not enough unique measurement paths through the structure to detect its relatively complex shape.

In contrast, there is a significant difference in the estimates of the moving objects. This can be seen by comparing Figure 5(b) and Figure 5(d). As expected from the analysis in Section 1.2, the variance-based method is only able to determine streaks where the moving object has been. If we instead consider the reconstruction provided by RETINA, it is apparent that RETINA has accurately and clearly detected the position of the moving objects.

In the second simulation, the 28 measuring nodes were placed randomly outside the imaging area and allowed to move slowly. The nodes moved according to a random velocity model such that they would pick a random velocity and travel at that velocity for a random duration. If they collided with either the boundaries of the network or the boundaries of the imaging area they would immediately pick a new velocity and duration. The velocity and duration were bounded such that nodes would move less than 0.1 units in each measurement interval. The current positions of all of the measurement nodes was assumed to be known by both RETINA and the variance-based algorithm. The reconstructed spatial loss fields after 400 measurement/movement iterations for the variance-based algorithm and RETINA are shown in Figure 6 along with the ending positions of the mobile measuring nodes.

The two reconstructions using the variance-based algorithm in Figure 6(a) and Figure 6(b) do not provide good estimates of either the static or dynamic aspects of the shadowing environment. While

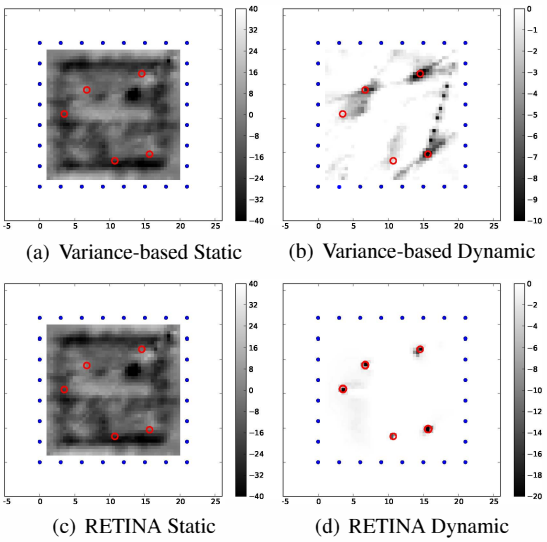

(a) Variance-based Static (b) Variance-based Dynamic

(c) RETINA Static (d) RETINA Dynamic

**Fig. 5**. Stationary Reconstruction Comparison

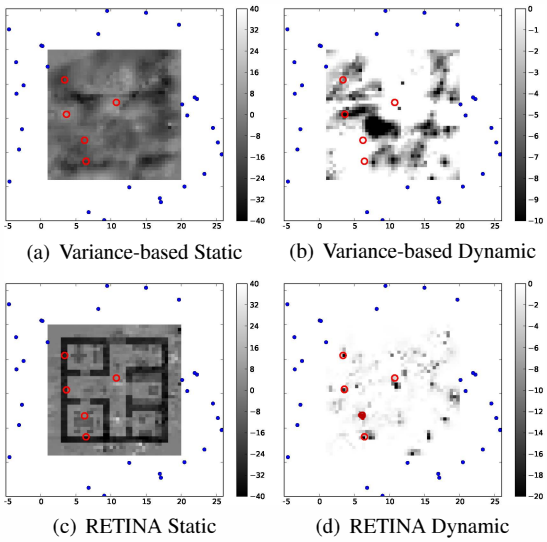

(a) Variance-based Static (b) Variance-based Dynamic

(c) RETINA Static (d) RETINA Dynamic

**Fig. 6**. Mobile Reconstruction Comparison

the analysis in Section 1.2 showed that this algorithm will perform poorly with mobile nodes, these results show that even slow movement can have catastrophic effects on the reconstruction.

The reconstructions based on the RETINA algorithm, on the other hand, perform much better. The reconstruction of the static portion of the environment in Figure 6(c) shows that instead of losing accuracy when the measurement nodes are mobile, RETINA is able to take advantage of the additional information provided by the slightly different paths to significantly increase its resolving power. The additional resolving power allows RETINA to achieve a reconstruction comparable to the actual spatial loss field from Figure 4. The RETINA reconstruction dynamic portion of the spatial loss field also works quite well. Due to the motion of the moving objects, the additional paths can not be used to increase the resolving power. In spite of this, it was still able to track all 5 moving objects, and only suffered a few extra reconstruction artifacts.

## 4. CONCLUSION

Received signal strength measurements commonly collected in ad-hoc wireless networks contain a significant amount of information about the physical characteristics of the network environment. Such information could be of enormous benefit in a wide range of applications. We have shown that recovering this information is a tomography problem and discussed the capabilities of existing methods. We then present a new algorithm, RF Exploitation for Tomographic Imaging and Non-cooperative Analysis (RETINA), capable of extracting information about both the static and dynamic components of the shadowing environment from RSS measurements. We have demonstrated through simulation that this algorithm is both more accurate and more robust than existing networks.

## 5. REFERENCES


[1] Ian F. Akyildiz, W. Su, Y. Sankarasubramaniam, and E. Cayirci, "Wireless sensor networks: a survey," *Computer Networks*, vol. 38, no. 4, pp. 393 – 422, 2002.

[2] L. L. Monte, L. K. Patton, and M. C. Wicks, "Direct-path mitigation for underground imaging in RF tomography," in *Proc. ICEAA*, 2010, pp. 27–30.

[3] M. C. Wicks, "RF tomography with application to ground penetrating radar," in *Proc. ACSSC*, 2007, pp. 2017–2022.

[4] Gabor T. Herman, *Fundamentals of Computerized Tomography: Image Reconstruction from Projections*, Springer, 2nd edition, 2009.

[5] J. Wilson and N. Patwari, "Regularization methods for radio tomographic imaging," in *Proc. Virginia Tech Wireless Symposium*, June 2009.

[6] J. Wilson and N. Patwari, "See-through walls: Motion tracking using variance-based radio tomography networks," *IEEE Trans. Mobile Comput.*, vol. 10, no. 5, pp. 612–621, 2011.

[7] J. Wilson and N. Patwari, "Radio tomographic imaging with wireless networks," *IEEE Trans. Mobile Comput.*, vol. 9, no. 5, pp. 621–632, 2010.

[8] Seung-Jun Kim, E. Dall'Anese, and G.B. Giannakis, "Cooperative spectrum sensing for cognitive radios using kriged Kalman filtering," *IEEE J. Sel. Topics Signal Process.*, vol. 5, no. 1, pp. 24 –36, Feb. 2011.

[9] Gordon L. Stüber, *Principles of Mobile Communications*, Kluwer Academic Publishers, 2nd edition, 2001.

[10] F. Graziosi and F. Santucci, "A general correlation model for shadow fading in mobile radio systems," *IEEE Commun. Lett.*, vol. 6, no. 3, pp. 102–104, 2002.

[11] M. Gudmundson, "Correlation model for shadow fading in mobile radio systems," *Electronics Letters*, vol. 27, no. 23, pp. 2145–2146, 1991.

[12] P. Agrawal and N. Patwari, "Correlated link shadow fading in multi-hop wireless networks," *IEEE Trans. Wireless Commun.*, vol. 8, no. 8, pp. 4024–4036, Aug. 2009.

[13] N. Patwari and P. Agrawal, "NeSh: A joint shadowing model for links in a multi-hop network," in *Proc. IEEE ICASSP*, 2008, pp. 2873–2876.

[14] S. Haykin, *Kalman Filters*, John Wiley & Sons, Inc., 2002.